Structural disorder versus chiral magnetism in $Cr_{1/3}NbS_2$

V. Dyadkin,[1, 2, *] F. Mushenok,[3, 4] A. Bosak,[5] D. Menzel,[6] S. Grigoriev,[2, 7] P. Pattison,[1] and D. Chernyshov[1]

[1] *Swiss-Norwegian Beamlines at the European Synchrotron Radiation Facility, 38000 Grenoble, France*
[2] *Petersburg Nuclear Physics Institute, RNC "Kurchatov institute", Gatchina, 188300 St-Petersburg, Russia*
[3] *Institute of Problems of Chemical Physics RAS, 142432 Chernogolovka, Russia*
[4] *School of Physics, University of Exeter, Stocker Road, Exeter, EX4 4QL, United Kingdom*
[5] *European Synchrotron Radiation Facility, 38000 Grenoble, France*
[6] *Institut für Physik der Kondensierten Materie, Technische Universität Braunschweig, D-38106 Braunschweig, Germany*
[7] *Saint-Petersburg State University, 198504 Saint-Petersburg, Russia*

(Dated: March 9, 2015)

arXiv:1503.01972v1 [cond-mat.mtrl-sci] 6 Mar 2015

The crystal structure of a disordered form of $Cr_{1/3}NbS_2$ has been characterized using diffraction and inelastic scattering of synchrotron radiation. In contrast to the previously reported symmetry ($P6_322$), the crystal can be described by a regular twinning of an average $P6_3$ structure with three disordered positions of the Cr ions. Short-range correlations of the occupational disorder result in a quite intense and structured diffuse scattering; a static nature of the disorder was unambiguously attributed by the inelastic x-ray scattering. The diffuse scattering has been modeled using a reverse Monte-Carlo algorithm assuming a disorder of the Cr sub-lattice only. The observed correlated disorder of the Cr sub-lattice reduces the temperature of the magnetic ordering from 130 K to 88 K and drastically modifies the field dependence of the magnetization as it is evidenced by the SQUID magnetometery. We conclude, that in contrast to the helicoidal spin structure assumed for $P6_322$ form, the compound under study is ferromagnetically ordered with a pronounced in-plane anisotropy.

PACS numbers: 75.40.-s, 75.25.+z, 61.05.cp, 61.05.fg, 75.50.Bb

I. INTRODUCTION

A lack of inversion symmetry in magnetic materials makes possible the antisymmetric Dzyaloshinsky-Moriya interaction (DMI) and results in a variety of magnetic phenomena. A chiral helicoidal order[1,2], skyrmion lattices[3,4], a quantum blue fog[5], a topological Hall effect[6], a first order phase transition driven by critical fluctuations[7] exemplify some of the topics attracting the attention of a wide range of physicists. An interesting and quite unusual circumstance is that, until recently, the most of the above listed phenomena have been proposed on the basis of the properties of MnSi and its substituted analogues. These compounds have a simple cubic crystal structure ($P2_13$ space group) with a unit cell which contains four metal and four silicon atoms in the 4a Wyckoff positions. The crystal structure is chiral in a sense that it does not coincide with its mirror image; for the ground state, and a certain part of the $(H-T)$ (magnetic field – temperature) phase diagram, the magnetic structure is also chiral and its chirality is unambiguously bound with the structural one[8,9]. Recently, the class of chiral magnets has been augmented with monogermanides of some 3d metals[10,11] and Cu_2OSeO_3[12–14], both having the same $P2_13$ space group as MnSi.

Another interesting example is the compound $Cr_{1/3}NbS_2$[15] where a chiral soliton lattice has been proposed for its magnetic structure[16]. Its hexagonal structure is built up from NbS_2 layers intercalated by Cr ions. There are three basic magnetic interactions which constitute the spin structure: (i) the ferromagnetic within the Cr layers $J_\perp$, (ii) another ferromagnetic one $J_\parallel$ and (iii) the DMI between Cr ions, the latter two interactions belong to the two intercalating layers separated by NbS_2[17]. The competition between the latter two interactions forms a helicoidal structure. Monte-Carlo simulations have recently shown[18] that the Cr ions are strongly ferromagnetically coupled in the (ab)-plane with $J_\perp \sim 74$ K, while they are weakly correlated between the layers with $J_\parallel \sim 10$ K and $D \sim 1.5$ K. The first constant $J_\perp$ determines solely the critical temperature of the compound, while the other two constants D and $J_\parallel$ balance in the length of the helix pitch.

At variance with the crystallographically well studied B20 silicides[19], the structural information on the other chiral magnets is rather incomplete and often limited to powder diffraction data. Thus, the absolute (chiral) sense has only been reported recently for both magnetism and crystal structure for Cu_2OSeO_3[14], this information is not yet available for $Cr_{1/3}NbS_2$ because the chirality cannot be characterized from powder diffraction. As far as we are aware, the atomic coordinates in $Cr_{1/3}NbS_2$ were measured only once, the refinement was done using nine neutron powder peaks and it was reported without any standard deviations[20]. Other experimental structural information is limited to the unit cell dimensions[17], and it is augmented with atomic coordinates borrowed from similar compounds[21]. In spite of the great interest in unusual and potentially technologically important properties, the understanding of a microscopic nature of the chiral magnetism calls for more complete and precise information on the underlaying crystal structure.

The compounds M_xNbS_2 (where M is a transition metal) are particularly interesting due to their layered hexagonal structure intercalated with transition metal ions. Layered NbS_2–based intercalates have revealed many fascinating phenomena including superconductivity together with charge and spin density waves[22,23], Fermi surface nesting effects[24,25], and also a structural disorder due to a distribution of the intercalated ions over several positions. M_xNbS_2 materials also show a variety of magnetic properties as a function of intercalated M and x:

- paramagnetic for intercalated Ti[20];
- previously reported as paramagnetic for V[20], but later on as ferromagnetic below $T_c = 50$ K and another unidentified magnetic phase below $T = 20$ K with $x = 1/3$[26];
- antiferromagnetic for Co with $T_N = 26$ K and for Ni with $T_N = 90$ K with $x = 1/3$[26–28];
- for Fe antiferromagnetic below $T_N = 150$ K with $x = 1/4$ and a spin-glass state below $T_g = 40$ K with $x = 1/3$[29,30];
- ferromagnetic and possible helicoidal state for Mn with $x = 1/3$ below $T_c = 42$ and with $x = 1/4$ below $T_c = 80$ K[31,32];
- helicoidal for Cr with $x = 1/3$ below $T_c = 130$ K[15,32].

In spite of the interest in the magnetic properties in $Cr_{1/3}NbS_2$[16], there is an unexpectedly large spread in the reported temperatures of the magnetic ordering; the published values vary from 100[33] to 132 K[34].

Here we revisit the intercalated crystal structure of the chiral helimagnet $Cr_{1/3}NbS_2$ using synchrotron radiation. All of the crystals we tested have a crystal structure which is indeed chiral but it is different from the one reported earlier. The crystal structure of $Cr_{1/3}NbS_2$ reveals a disorder in the Cr sub-lattice; the presence of disorder has also been confirmed in a separate diffuse scattering measurement. The nature of the observed diffuse component relates to short-range correlations and, as evidenced by the inelastic x-ray scattering experiment (IXS), shows the elastic peak to be the major contributor of the characteristic diffuse scattering.

The magnetic susceptibility measured with SQUID magnetometery shows $T_c \approx 88$ K, such a low value points to a link between the structural disorder and magnetic properties. Magnetization as a function of both field and temperature also differs from the data presented earlier[32], and expected from the theoretical consideration of helicoidal magnets[15]. Taken together, the new data call for a revision of theoretical models for chiral magnetic interactions to include effects of disorder and short range correlations in spatial distribution of magnetic centers. Moreover, the attribution of the given magnetic transition to the stoichiometry and disorder pattern might imply the revision of the data for other intercalates.

II. EXPERIMENTAL

A. Sample preparation

A polycrystalline $Cr_{1/3}NbS_2$ sample was prepared by sintering of the mixture of starting components at 800° in vacuum. The $Cr_{1/3}NbS_2$ single crystals were grown using chemical transport method in iodine atmosphere at the temperature gradient $T = 950$ — 800 °C. The obtained crystals had a natural faceting and a metallic luster. The chemical composition has been independently checked with the Energy Dispersive X-Ray Analysis (EDX), with two randomly selected crystals and probing different spots. The results are very homogeneous with Cr/Nb ratio ~ 0.3.

B. X-ray Scattering Experiments

Single crystal Bragg diffraction data were collected at the room temperature using the PILATUS@SNBL diffractometer at the BM01A end station of the Swiss-Norwegian Beamlines at the ESRF (Grenoble, France); the wavelength of the synchrotron radiation was set to 0.68290 Å. The data were collected with a single ϕ-scan with angular step of 0.1° in a shutter-free mode with the PILATUS2M detector.

The raw data were processed with the SNBL Toolbox, the integral intensities were extracted from the frames with the CrysAlisPro software[35], the crystal structure was solved with SHELXS and refined with SHELXL[36].

Single crystal data on diffuse scattering have been measured at room temperature using the PILATUS6M detector at the ID23 (ESRF, Grenoble, France) with 0.689 Å wavelength and 0.1° slicing. The maps of reciprocal space were recovered from the raw frames using in-house software with the orientation matrix as refined in CrysAlisPro. The diffuse scattering data were modeled with a reverse Monte-Carlo algorithm as implemented in the in-house software using structural models found from the Bragg scattering experiment.

The IXS measurement was carried out at the beamline ID28 at the ESRF. The spectrometer was operated at 17.794 keV incident energy, providing an energy resolution of 3.0 meV full-width-half-maximum (Si(999) reflection). IXS scans were performed in transmission geometry along selected directions in reciprocal space. Further details of the experimental set-up and the data treatment can be found elsewhere[37].

C. SQUID magnetometery

The magnetization of a single crystal sample was measured using SQUID magnetometer (Quantum Design MPMS-5S). Temperature dependent measurements were performed in the range of 2 – 300 K. The field dependent magnetization was obtained in a field range from

$H = -5$ to 5 T at $T = 6$ K. The magnetic field was applied in two different orientations relative to the crystallographic directions parallel to the c-axis and within the ab-plane perpendicular to c. The magnetic moment per Cr atom has been calculated from the mass and the stoichiometry of the crystal based on the EDX data.

III. RESULTS

A. Magnetic properties

The magnetization curves at $T = 6$ K for $H \parallel c$ and $H \perp c$ show an anisotropic behavior (Fig. 1) which differs significantly from the one of the canonical $CrNbS_2$[38]. For $H \parallel c$ the magnetization curve consists of two regimes: at low fields up to $H \approx 0.1$ T the magnetization increases rapidly from 0 to 0.5 μ_B/Cr. At higher fields the magnetization grows smoothly up to $1.2\mu_B$ at 5 T. Fast saturation of magnetization for H within the ab-plane and slow increase for $H \parallel c$ are typical features of magnetic materials with uniaxial easy-plane anisotropy. For $H \perp c$ the saturation field equals to 50 mT which is below the range reported previously (from 1.5 kOe[32] to 2 kOe[16]). The saturation magnetic moment $M_S = 1.3\mu_B$ per Cr ion is considerably lower than the spin-only value of $3\mu_B$ per Cr^{3+} ions with $S = 3/2$. It is most likely that the reduction of the saturation moment is caused by delocalization of the d-electrons of Cr^{3+}.

The coercivity is smaller than 1 mT for both orientations. This value, however, is comparable with a residual magnetic field of the SQUID magnetometer and, therefore, the coercivity is below the experimental error. The negligibly small remanent magnetization and coercivity for $H \perp c$ can be explained by a continous spin rotation in the basal plane towards the external field direction. Along the c-axis, the field induces a canting of the spins competing against the easy-plane anisotropy.

For $H \parallel c$ a linear $M(H)$ dependence would be expected in uniaxial easy-plane ferromagnets. However, a non-linear $M(H)$ dependence is observed for the studied crystals which suggests that not only uniaxial anisotropy has to be taken into account in order to describe the magnetization behavior. Most likely, also the non-uniform distribution of the intercalated chromium ions plays an important role.

The temperature dependent magnetization at small magnetic fields (2.5 to 100 mT) well below saturation shows for both field orientations magnetic order below approx. 90 K (Fig. 2). The increasing field leads to an increase of the magnetization, while the moment is smaller along the c-axis than within the ab-plane. This is also reflected by the anisotropic magnetization curves in Fig. 1.

Arrott plots have been used to eliminate the influence of the external magnetic field and to accurately determine the ordering temperature. According to the mean field theory[39], a plot of M^2 versus H/M for different

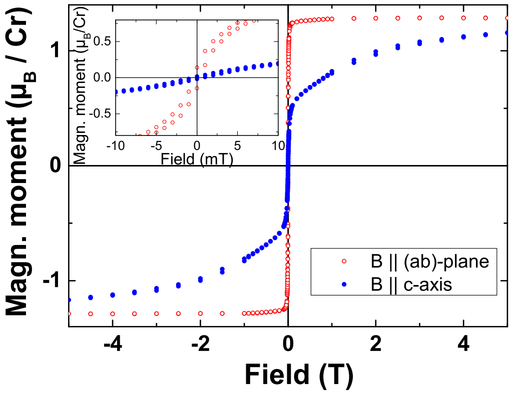

FIG. 1. Magnetization curves for $H \parallel ab$ and $H \parallel c$ at $T = 6$ K.

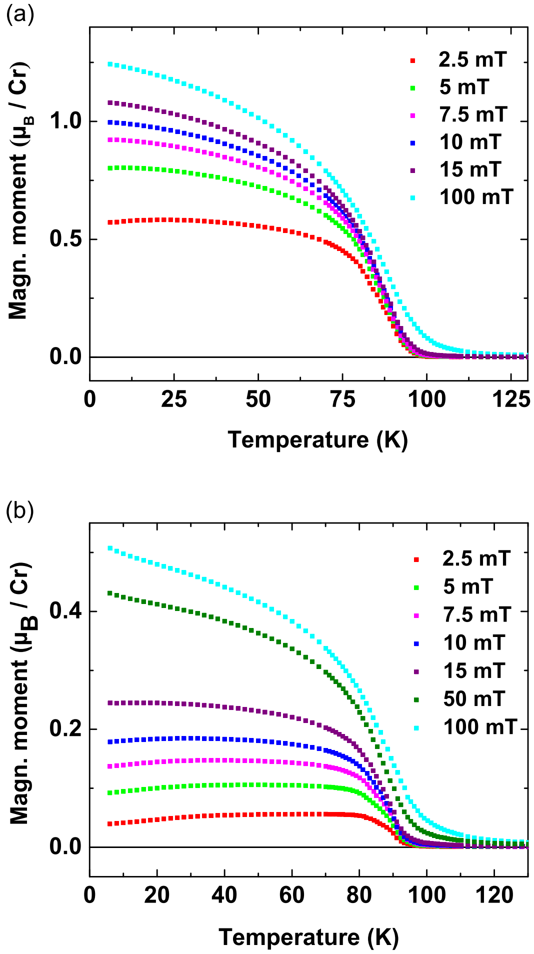

FIG. 2. Temperature dependent magnetization for (a) $H \parallel ab$ and (b) $H \parallel c$ for different magnetic fields.

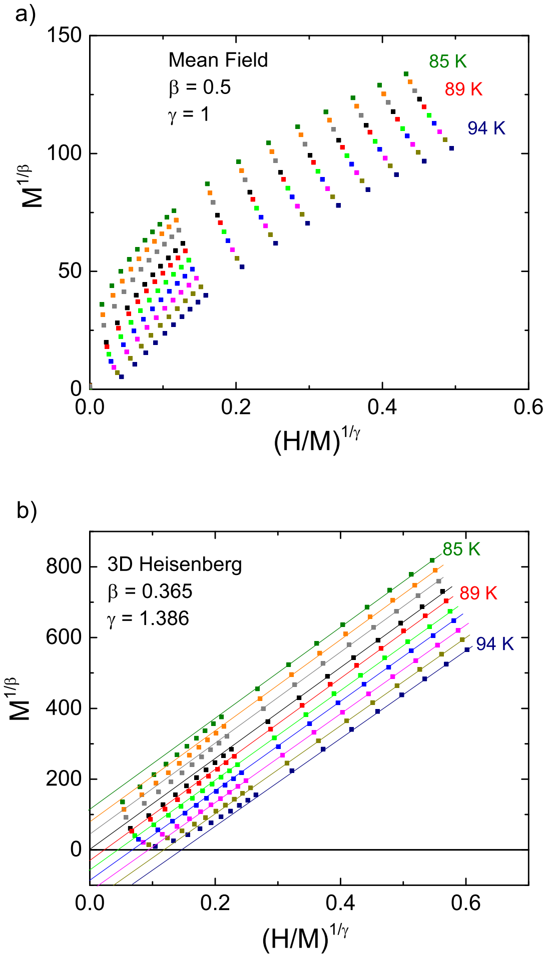

FIG. 3. Arrot plots for $H \parallel ab$-plane according to (a) a mean-field model ($\beta = 0.5$, $\gamma = 1$) and (b) a 3D Heisenberg model ($\beta = 0.365$, $\gamma = 1.336$).

temperatures should show a linear dependence in the large field range. However, all curves are non-linear, but show a downward curvature (Fig. 3a). Therefore, we modified the Arrott plot taking the critical exponents into account[40]. A plot of $M^{1/\beta}$ versus $(H/M)^{1/\gamma}$ is shown in Fig. 3b with the critical exponents along a 3D-Heisenberg model ($\beta = 0.365$, $\gamma = 1.336$)[41] representing all linear behavior at high fields. From extrapolation of the slopes we obtain an ordering temperature of $T_C = 88$ K which is significantly smaller than reported in[15,32]. The critical exponents fulfill the Widom scaling relation $\delta = 1 + \gamma/\beta$[42], which gives $\delta = 4.697$ for the experimental data when the field dependence of the magnetization is considered as $M \propto H^{1/\delta}$ at $T = T_C$. This result agrees well with $\delta = 4.797$ according to the 3D Heisenberg model in contrast to $\delta = 3$ which would hold for a mean-field model.

TABLE I. Three possible structural models for $Cr_{1/3}NbS_2$. SG is the space group, WP is the Wykoff positions.

Model	SG	R_1	R_w	Cr WP	Cr/Nb Ratio
I	$P6_322$	0.148	0.29	$2c$	0.333, fixed by symmetry
II	$P6_322$	0.044	0.14	$2c$, $2b$	0.4
III	$P6_3$	0.015	0.044	$2b$, $2a$	0.314

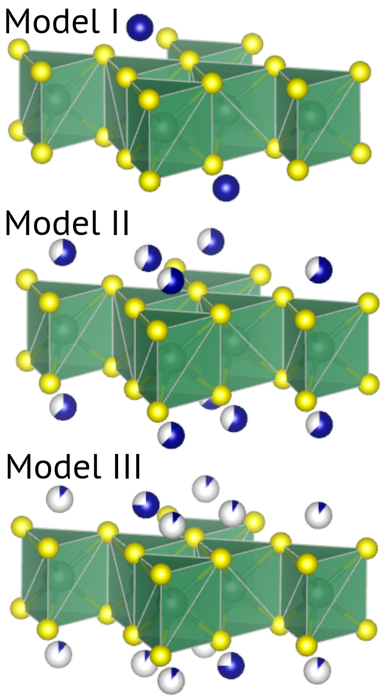

FIG. 4. Fragment of crystal structures for the models I, II, III. The occupancy of disordered Cr sites is encoded as a colored sector.

B. Bragg diffraction and crystal structure

Bragg data were indexed with a hexagonal cell ($a = 5.738(5)$ Å, $b = 5.738(5)$ Å, $c = 12.018(5)$ Å) in a close agreement with the unit cell dimensions reported previously. Three models have been tested for the crystal structure, as compared in Table I and Figure 4. The model I was proposed for the crystal structure of $Cr_{1/3}NbS_2$ with space group $P6_322$ and the atomic positions set close to those reported in Ref. 17, Cr ion occupies the $2c$ Wyckoff position. The refinement gives rather high R-factors, and analysis of the residual electron density reveals additional maxima not accounted by the model.

Model II includes an additional maximum at the $2b$ Wyckoff position which indicate presence of a disordered Cr ion. Disordered $M_{1/3}NbS_2$ (where M is Mn, Fe, Co, Ni, V) has been reported, but the additional maxima were located at $2a$ and $2d$ and the positions are found to be only slightly populated[43]. Refinement with the model II has an acceptable quality, with, however, a few warn-

TABLE II. Crystal data for $P6_3$ (model III).

Empirical formula	$Cr_{0.314}NbS_2$
Temperature	293 K
Wavelength	0.68290 Å
Crystal system, space group	hexagonal, $P6_3$
Unit cell dimensions	$a = 5.738(5)$ Å
	$b = 5.738(5)$ Å
	$c = 12.018(5)$ Å
Theta range for data collection	1.63° to 25.25°
Limiting indices	$-7 <= h <= 7$,
	$-6 <= k <= 6$,
	$-15 <= l <= 15$
Reflections collected / unique	2050 / 466 [$R_{\text{int}} = 0.0198$]
Completeness to theta = 25.25	98.8

ing signs: (i) analysis of a variance of reflections included into the refinement indicates a possible twinning; (ii) the refined value of Cr content is higher than the measured with EDX (the Cr/Nb ratio is expected to be 1/3, measured is 0.3, refined is 0.4).

Therefore, the Model III, which has the $P6_3$ symmetry and the twinning law 010 100 00$\bar{1}$, has been proposed. The Cr ions are found to be disordered over three independent crystallographic positions. The refinement gives the lowest R-factors and the refined composition is close to the expected and measured with the Cr/Nb ratio around 0.314. Corresponding crystal data and results of the refinement at the room temperature are summarized in Tables I and II and structural parameters are available as crystallographic information file (CIF) in supplementary materials.

C. Diffuse scattering and structural disorder

Diffuse scattering has a form of a honeycomb structure extended along c^*, the walls of honeycomb cells are weakly modulated along this direction (Fig. 5). Bragg nodes stay in the centers of honeycomb cells. Along c^* the nodes are connected by the diffuse streaks which points to the presence of 2D structural defects parallel to the NbS_2 planes; they can be interpreted as the boundaries between the twins.

D. Inelastic x-ray scattering

Energy transfer scans along a wall of the honeycomb is shown at Fig. 6. The intensity of the elastic peak follows the intensity of the diffuse component, while no substantial inelastic signal can be seen beyond. That confirms essentially elastic character of the observed scattering and therefore static nature of the underlaying disorder.

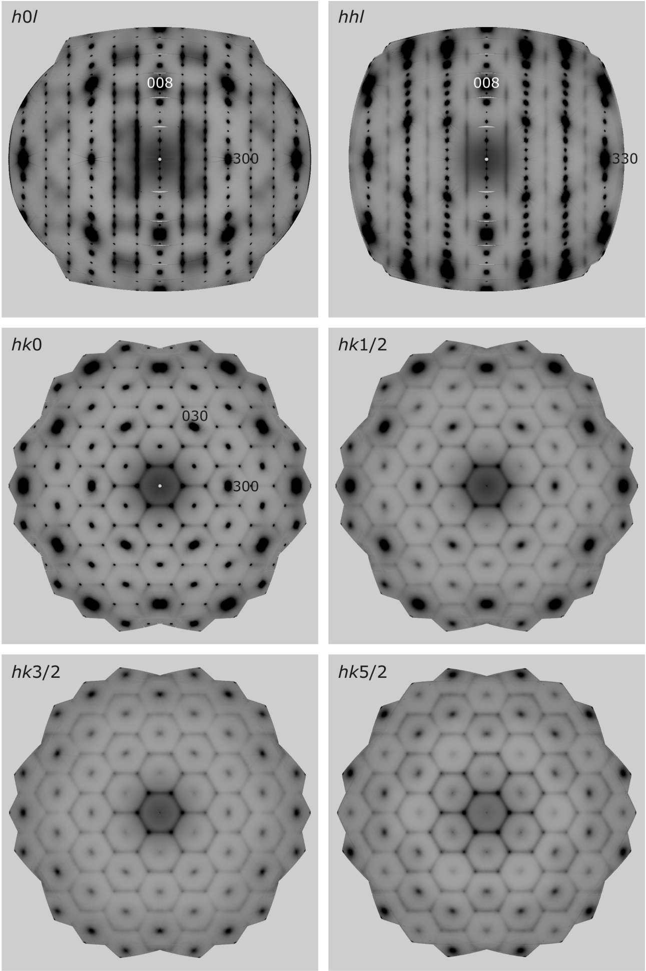

FIG. 5. Maps of the diffuse scattering for different layers in reciprocal space.

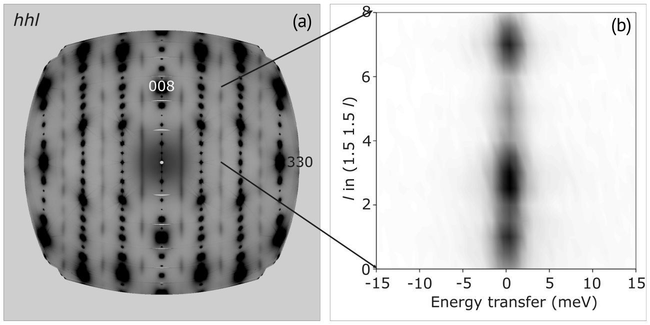

FIG. 6. (a) The hhl-section of reciprocal space; (b) (E, Q) intensity map for the region of interest indicated in (a).

E. Monte-Carlo modeling of the disordered structure

Diffuse scattering has been modeled using the Reverse Monte-Carlo method (RMC) based on the Model II and using only one partially occupied Cr site (application of the twinned Model III was difficult because the number

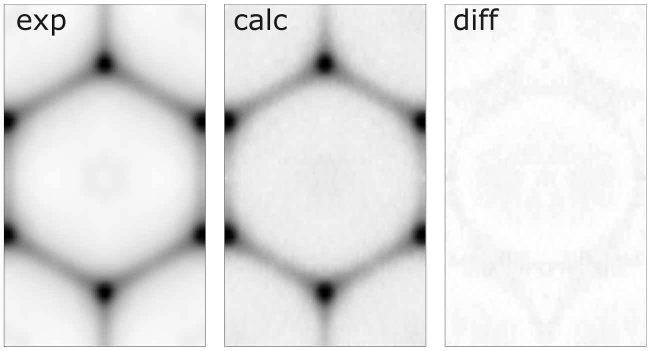

FIG. 7. Diffuse scattering patterns: (exp) symmetrized experimental, (calc) resilting from the RMC, (diff) difference map. The same intensity scale is used.

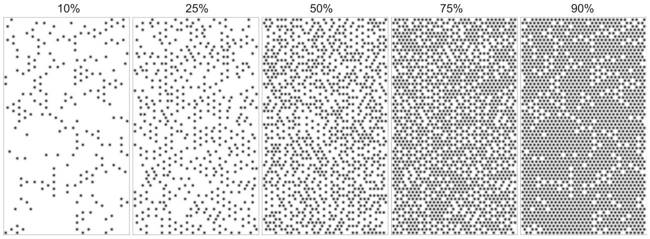

FIG. 8. Randomly chosen *xy*-sections of the model clusters with the given Cr content.

of correlating parameters was too large).

The RMC simulation was performed on a cluster $32 \times 32 \times 32$ atoms to profit the efficiency of the fast Fourier transform. In an initial configuration the lattice sites were randomly occupied with a predefined concentration. Each simulation step included:

1. a swap between randomly chosen vacancy and atom;
2. calculation of the scattering intensities together with adjustment of the background and scaling factor (c^* dependence was removed by the averaging);
3. calculation of χ^2 and acceptance or rejection of the swap.

For the given cluster size, a reasonable convergence (Fig. 7) is achieved in $\sim 10^5$ steps. As c^* correlations were neglected, inspection of any XY section of converged cluster is illustrative enough. Qualitatively, one could summarize the message as follows: vacancies/atoms are distributed in a way to minimize contacts between the neighbors of the same type, locally resulting in a loss of hexagonal packing (Fig. 8).

IV. DISCUSSION AND CONCLUSION

Our results, from both Bragg and diffuse scattering unambiguously indicate that we are dealing with a disordered form of the title compound. Notably, the crystal structure of this chiral helimagnet has never been accurately probed before with a single crystal diffraction experiment; we cannot, therefore, surely state that the disordered structure we observe is a generic one. However, the magnetic ordering temperature is reported inconsistently in the literature, which strongly suggests the necessity of a careful structural characterization in order to validate the real structure of the material under study.

We show that the correct symmetry is indeed chiral, but it is lower than the reported before. The $P6_3$ structure is twinned and disordered with respect to the Cr sublattice, which provides most of resonant contribution. As a result, the Flack parameter of the entire structure is not well defined. In contrast to MnSi[8] and Cu_2OSeO_3[14] the absolute structure cannot be reliably determined from the crystals tested in the present study.

The crystal structure of the new form is almost identical to the previously reported ones in terms of the geometry of the NbS_2 fragment. The main difference to the previously proposed structural model ($P6_322$) is a disorder in Cr layers. In contrast to the initially expected $P6_322$ structure that assumes only one position for the Cr ions, the experimentally observed $P6_3$ symmetry offers three Wyckoff positions with independent occupancies. Unconstrained refinement of the occupancies results in $Cr_{0.314}NbS_2$, that is reasonably close to the stoichiometric composition.

The disorder found in the magnetic Cr sub-lattice is not random but correlated and results in the honeycomb-like diffuse scattering shown to be essentially elastic by IXS. This pattern suggests a tendency towards the clustering of Cr ions in hexagonal fragments within the layers. Interlayer correlations are manifested in the form of modulated diffuse rods propagating along c^*. Such a specific correlated disorder should strongly affect magnetic ordering, in particular, the ordering temperature; more experiments on diffuse scattering combined with magnetization measurements are needed to clarify an interplay between the correlated disorder and magnetic properties.

We conclude with a note on the necessity of further revision of crystal structure of the chiral magnets. A chiral long-range magnetic spiral (hundreds or even thousands of Angstroms) is a giant object and it should not necessarily recognize the chirality of the few Angstroms size crystal unit cell. This is the case in rare-earth magnets like Ho, where the hexagonal structure is achiral and centrosymmetric but the magnetic ordering is chiral and its chirality can be changed by an external impact[44]. However, in the case of chiral magnets with a chiral crystal structure, as it was shown for B20 magnets[45,46], the atomic arrangement in a unit cell unambiguously dictates how the giant magnetic spiral must twist. This chiral coupling can be mapped phenomenologically by the Dzyaloshinsky-Moriya interaction, a microscopic mechanism behind it is still to be uncovered. Thus, the same link has been seen for both metals[8] and insulators[14] indicating that it is not related to the conduction electrons. In the 3d-metal monogermanides the link changes its sign as a function of chemical composition, that points out the role of 3d-electrons[47,48] and, possibly, geometric factors related to the ionic radii[49]. The results we present here indicate that a disorder could also affect the chiral magnetism and illustrate that not only the average structure but also local deviations from it may influence the magnetic properties.

V. ACKNOWLEDGEMENTS

The authors are indebted to I. Snigireva (ESRF) for her help with the EDX analysis and A. Popov (ESRF) for the assistance with the diffuse scattering data collection at the ID27 beamline. We would also like to thank V. Dmitriev (SNBL) for fruitful discussions. FM was supported by the grant MK1474.2014.3 for young scientist.

---

[*] diadkin@esrf.fr

[1] P. Båk and M. H. Jensen, J. Phys. C **13**, L881 (1980).

[2] S. V. Maleyev, Phys. Rev. B **73**, 174402 (2006).

[3] S. Mühlbauer, B. Binz, F. Jonietz, C. Pfleiderer, A. Rosch, A. Neubauer, R. Georgii, and P. Böni, Science **323**, 915 (2009).

[4] X. Z. Yu, Y. Onose, N. Kanazawa, J. H. Park, J. H. Han, Y. Matsui, N. Nagaosa, and Y. Tokura, Nature **465**, 901 (2010).

[5] S. Tewari, D. Belitz, and T. R. Kirkpatrick, Phys. Rev. Lett. **96**, 047207 (2006).

[6] R. Ritz, M. Halder, C. Franz, A. Bauer, M. Wagner, R. Bamler, A. Rosch, and C. Pfleiderer, Phys. Rev. B **87**, 134424 (2013).

[7] S. M. Stishov, A. E. Petrova, A. A. Shikov, T. A. Lograsso, E. I. Isaev, B. Johansson, and L. L. Daemen, Phys. Rev. Lett. **105**, 236403 (2010).

[8] S. V. Grigoriev, D. Chernyshov, V. A. Dyadkin, V. Dmitriev, S. V. Maleyev, E. V. Moskvin, D. Menzel, J. Schoenes, and H. Eckerlebe, Phys. Rev. Lett. **102**, 037204 (2009).

[9] V. A. Dyadkin, S. V. Grigoriev, D. Menzel, D. Chernyshov, V. Dmitriev, J. Schoenes, S. V. Maleyev, E. V. Moskvin, and H. Eckerlebe, Phys. Rev. B **84**, 014435 (2011).

[10] N. Kanazawa, J.-H. Kim, D. S. Inosov, J. S. White, N. Egetenmeyer, J. L. Gavilano, S. Ishiwata, Y. Onose, T. Arima, B. Keimer, and Y. Tokura, Phys. Rev. B **86**, 134425 (2012).

[11] V. Dyadkin, S. Grigoriev, S. V. Ovsyannikov, E. Bykova, L. Dubrovinsky, A. Tsvyashchenko, L. Fomicheva, and D. Chernyshov, Acta Cryst. B **70**, 676 (2014).

[12] S. Seki, J.-H. Kim, D. S. Inosov, R. Georgii, B. Keimer, S. Ishiwata, and Y. Tokura, Phys. Rev. B **85**, 220406 (2012).

[13] T. Adams, A. Chacon, M. Wagner, A. Bauer, G. Brandl, B. Pedersen, H. Berger, P. Lemmens, and C. Pfleiderer, Phys. Rev. Lett. **108**, 237204 (2012).

[14] V. Dyadkin, K. Prša, S. V. Grigoriev, J. S. White, P. Huang, H. M. Rønnow, A. Magrez, C. D. Dewhurst, and D. Chernyshov, Phys. Rev. B **89**, 140409 (2014).

[15] T. Moriya and T. Miyadai, Solid State Commun. **42**, 209 (1982).

[16] Y. Togawa, T. Koyama, K. Takayanagi, S. Mori, Y. Kousaka, J. Akimitsu, S. Nishihara, K. Inoue, A. S. Ovchinnikov, and J. Kishine, Phys. Rev. Lett. **108**, 107202 (2012).

[17] T. Miyadai, K. Kikuchi, H. Kondo, S. Sakka, M. Arai, and Y. Ishikawa, J. Phys. Soc. Jpn. **52**, 1394 (1983).

[18] M. Shinozaki, S. Hoshino, J. Kishine, K. Hukushima, and Y. Kato, in *Japan-Russia International Research Symposium on Chiral Magnetism, 6th-8th December 2014, Hiroshima (Japan)* (2014) p. Abstract O04.

[19] V. Dmitriev, D. Chernyshov, S. Grigoriev, and V. Dyadkin, J. Phys.: Condens. Matter **24**, 366005 (2012).

[20] F. Hulliger and E. Pobitschka, J. Solid State Chem. **1**, 117 (1970).

[21] J. Rouxel, A. L. Blanc, and A. Royer, Bulletin de la Societe Chimique de France **1971**, 2019 (1971).

[22] I. Guillamón, H. Suderow, S. Vieira, L. Cario, P. Diener, and P. Rodière, Phys. Rev. Lett. **101**, 166407 (2008).

[23] V. G. Tissen, M. R. Osorio, J. P. Brison, N. M. Nemes, M. García-Hernández, L. Cario, P. Rodière, S. Vieira, and H. Suderow, Phys. Rev. B **87**, 134502 (2013).

[24] C. Battaglia, H. Cercellier, L. Despont, C. Monney, M. Prester, H. Berger, L. Forr, M. G. Garnier, and P. Aebi, EPJ B **57**, 385 (2007).

[25] D. S. Inosov, V. B. Zabolotnyy, D. V. Evtushinsky, A. A. Kordyuk, B. Bchner, R. Follath, H. Berger, and S. V. Borisenko, New J. Phys. **10**, 125027 (2008).

[26] R. H. Friend, A. R. Beal, and A. D. Yoffe, Philos. Mag. **35**, 1269 (1977).

[27] S. S. P. Parkin and R. H. Friend, Philos. Mag. B **41**, 65 (1980).

[28] S. S. P. Parkin, E. A. Marseglia, and P. J. Brown, Journal of Physics C: Solid State Physics **16**, 2765 (1983).

[29] T. Tsuji, Y. Yamamura, M. Koyano, S. Katayama, and M. Ito, J. Alloy. Compd. **317318**, 213 (2001).

[30] Y. Yamamura, S. Moriyama, T. Tsuji, Y. Iwasa, M. Koyano, S. Katayama, and M. Ito, J. Alloy. Compd. **383**, 338 (2004).

[31] K. Miwa, H. Ikuta, H. Hinode, T. Uchida, and M. Wakihara, J. Solid State Chem. **125**, 178 (1996).

[32] Y. Kousaka, Y. Nakao, J. Kishine, M. Akita, K. Inoue, and J. Akimitsu, Nucl. Instrum. Meth. A **600**, 250 (2009).

[33] F. B. Mushenok, EPJ B **86**, 1 (2013).

[34] Y. Togawa, Y. Kousaka, S. Nishihara, K. Inoue, J. Akimitsu, A. S. Ovchinnikov, and J. Kishine, Phys. Rev. Lett. **111**, 197204 (2013).

[35] Agilent Technology, "Agilent Technologies UK Ltd., Oxford, UK, CrysAlisPro Software system, Version 1.171.36.28," (2013).

[36] G. M. Sheldrick, Acta Crystallogr. Sect. A **64**, 112 (2008).

[37] M. Krisch and F. Sette, in *Light Scattering in Solid IX*, Topics in Applied Physics, Vol. 108, edited by M. Cardona and R. Merlin (Springer Berlin Heidelberg, 2007) pp. 317–370.

[38] N. J. Ghimire, M. A. McGuire, D. S. Parker, B. Sipos, S. Tang, J.-Q. Yan, B. C. Sales, and D. Mandrus, Phys. Rev. B **87**, 104403 (2013).

[39] S. A. Brazovskii, Sov. Phys. JETP **41**, 85 (1975).

[40] M. E. Fisher, Rep. Prog. Phys. **30**, 615 (1967).

[41] L. Zhang, J. Fan, L. Li, R. Li, L. Ling, Z. Qu, W. Tong, S. Tan, and Y. Zhang, EPL **91**, 57001 (2010).

[42] L. Kadanoff, Physics **2**, 263 (1966).

[43] B. V. Laar, H. Rietveld, and D. Ijdo, J. Solid State Chem. **3**, 154 (1971).

[44] V. P. Plakhty, W. Schweika, T. Brückel, J. Kulda, S. V. Gavrilov, L.-P. Regnault, and D. Visser, Phys. Rev. B **64**, 100402 (2001).

[45] S. V. Grigoriev, D. Chernyshov, V. A. Dyadkin, V. Dmitriev, E. V. Moskvin, D. Lamago, T. Wolf, D. Menzel, J. Schoenes, S. V. Maleyev, and H. Eckerlebe, Phys. Rev. B **81**, 012408 (2010).

[46] V. Dyadkin, S. Grigoriev, D. Menzel, E. Moskvin, S. Maleyev, and H. Eckerlebe, Physica B **406**, 2385 (2011).

[47] S. V. Grigoriev, N. M. Potapova, S.-A. Siegfried, V. A. Dyadkin, E. V. Moskvin, V. Dmitriev, D. Menzel, C. D. Dewhurst, D. Chernyshov, R. A. Sadykov, L. N. Fomicheva, and A. V. Tsvyashchenko, Phys. Rev. Lett. **110**, 207201 (2013).

[48] S. V. Grigoriev, S.-A. Siegfried, E. V. Altynbayev, N. M. Potapova, V. Dyadkin, E. V. Moskvin, D. Menzel, A. Heinemann, S. N. Axenov, L. N. Fomicheva, and A. V. Tsvyashchenko, Phys. Rev. B **90**, 174414 (2014).

[49] V. A. Chizhikov and V. E. Dmitrienko, Phys. Rev. B **88**, 214402 (2013).